



OPEN

## Oxidative stress monitoring in iPSC-derived motor neurons using genetically encoded biosensors of H<sub>2</sub>O<sub>2</sub>

Elizaveta Ustyantseva<sup>1✉</sup>, Sophia V. Pavlova<sup>1,2,3</sup>, Anastasia A. Malakhova<sup>1,2,3</sup>, Kirill Ustyantsev<sup>1</sup>, Suren M. Zakian<sup>1,2,3</sup> & Sergey P. Medvedev<sup>1,2,3✉</sup>

Oxidative stress plays an important role in the development of neurodegenerative diseases, being either the initiator or part of a pathological cascade that leads to the neuron's death. Genetically encoded biosensors of oxidative stress demonstrated their general functionality and overall safety in various systems. However, there is still insufficient data regarding their use in the research of disease-related phenotypes in relevant model systems, such as human cells. Here, we establish an approach for monitoring the redox state of live motor neurons with *SOD1* mutations associated with amyotrophic lateral sclerosis. Using CRISPR/Cas9, we insert genetically encoded biosensors of cytoplasmic and mitochondrial H<sub>2</sub>O<sub>2</sub> in the genome of induced pluripotent stem cell (iPSC) lines. We demonstrate that the biosensors remain functional in motor neurons derived from these iPSCs and reflect the differences in the stationary redox state of the neurons with different genotypes. Moreover, we show that the biosensors respond to alterations in motor neuron oxidation caused by either environmental changes or cellular stress. Thus, the obtained platform is suitable for cell-based research of neurodegenerative mechanisms.

Redox reactions are part of cellular metabolism. Generally, reactive oxygen species (ROS), emerging as a byproduct of such reactions, are quickly neutralized by antioxidant systems<sup>1</sup>. In oxidative stress, ROS accumulate due to excessive production or disturbed utilization, leading to cell malfunction<sup>2</sup>. An increasing number of ROS molecules alters protein structure, changes properties of membranes due to lipid peroxidation, and causes DNA damage, which makes oxidative stress one of the major mechanisms of degenerative disorders and aging<sup>3,4</sup>.

Oxidative stress is known to play an important role in various pathologies, and its involvement in the development of neurodegenerative diseases is undeniable, although not always clear<sup>5,6</sup>. Indeed, oxidative stress is strongly associated with amyotrophic lateral sclerosis (ALS)—a disorder characterized by the inevitable death of motor neurons (MNs) leading to progressive paralysis<sup>7</sup>. The first ALS-associated gene, *SOD1*, encoding the antioxidant protein superoxide dismutase 1, was discovered in 1993; thus, oxidative stress has been proposed as the primary pathological mechanism of the disease<sup>8</sup>. However, subsequent studies revealed that ALS has a much more complex etiology involving other genes and that only 10% of cases are hereditary<sup>9–11</sup>. Nonetheless, signs of oxidative damage have been found in both patients and model organisms, regardless of the initial cause of the disease, suggesting a universal role of redox imbalance in MN damage<sup>12–14</sup>.

Redox studies are often conducted by measuring key molecules, including but not limited to glutathione (GSH/GSSG), hydrogen peroxide (H<sub>2</sub>O<sub>2</sub>), and NADP<sup>+</sup>/NADPH<sup>15,16</sup>. Although dozens of molecular chemical probes have been developed for such analyses, most have low specificity and availability and interfere with cellular processes<sup>17,18</sup>. Genetically encoded biosensors can be applied for the same measurement as molecular probes<sup>19</sup>. These protein-based detectors are initially delivered inside the cell in the form of nucleic acid. The cell subsequently produces biosensor molecules as long as the coding sequence is available. Since the biosensor molecules are produced inside the cell, they are not limited by availability and, therefore, can be applied not only in cell culture but also in more complex model systems, such as animals or plants<sup>20–22</sup>. Furthermore, the

<sup>1</sup>The Federal Research Center Institute of Cytology and Genetics, Siberian Branch of Russian Academy of Sciences, 10, Lavrentiev Ave, 630090 Novosibirsk, Russia. <sup>2</sup>Institute of Chemical Biology and Fundamental Medicine, Siberian Branch of the Russian Academy of Sciences, 8, Lavrentiev Ave., 630090 Novosibirsk, Russia. <sup>3</sup>E. Meshalkin National Medical Research Center of the Ministry of Health of the Russian Federation, 15 Rechkunovskaya Str., 630055 Novosibirsk, Russia. ✉email: e.ustyantseva21@gmail.com; medvedev@bionet.nsc.ru

nature of genetically encoded biosensors allows for easy modifications, such as the addition of signal peptides that direct the biosensor to specific cellular compartments (nucleus, mitochondria, endoplasmic reticulum, and plasma membrane)<sup>23,24</sup>. Traditional methods for research with genetically encoded biosensors in cell culture imply transient expression via plasmid delivery or viral-mediated integration of the biosensors sequences<sup>4</sup>. The first approach provides a high-intensity signal but does not allow long-term experiments since the plasmid copy number reduces by half with every cell division. The second method, by contrast, provides a stable expression of the biosensor but does not guarantee reliable results since randomly integrated biosensors can disturb genome function<sup>25</sup>. Although many redox biosensors have been developed in recent years, only a few have been validated in model systems as suitable for studying disease-associated phenotypes<sup>20,26–28</sup>.

Here, we developed a platform for monitoring oxidative stress in live MNs using reduction–oxidation sensitive green fluorescent protein 2 (roGFP2)-based biosensors differentially targeted to the cytoplasm (Cyto-roGFP2-Orp1) and mitochondria (Mito-roGFP2-Orp1). These are well-known ratiometric biosensors that reflect H<sub>2</sub>O<sub>2</sub> level, hence, *relative* oxidation in the respective cellular compartments<sup>29</sup>. First, to create a basis for our research, we generated isogenic induced pluripotent stem cell (iPSC) lines with mutations affecting different parts of the ALS-associated *SOD1* gene. Next, we allocated the biosensors sequences in the “safe harbor” *AAVS1* locus of these iPSC lines under the control of the Tet-On doxycycline-inducible expression system. This approach allowed us not only to avoid the potential adverse effect of the insert but also to generate cell lines with a stable yet controllable expression of the biosensors. Finally, we assessed the functionality of the biosensors in MNs, derived from the generated iPSCs, and showed that they reflect changes in the oxidation of these cells in conditions of direct increase of ROS in the cellular environment, as well as during neuronal-specific glutamate-induced stress. Thus, this platform can serve as an adequate model to study redox-associated pathologies in neurodegenerative diseases.

## Results

**Introduction of the *SOD1* D91A and G128R mutations in iPSCs of the clinically healthy donor.** The *SOD1* gene has more than 140 mutations associated with ALS, which define the clinical features of the disease such as its manifestation age, rate of progression, presence of additional symptoms, etc.<sup>30</sup>. We chose c.272A>C and c.382G>C mutations that lead to either a relatively benign or severe disease course, respectively<sup>31,32</sup>. In the first step of our workflow (Fig. 1A), we designed corresponding CRISPR/Cas9 guide RNA targeting the sequences in the exons 4 and 5 of *SOD1* and single-stranded oligodeoxynucleotides (ssODN) donor templates necessary for the introduction of c.272A>C and c.382G>C single-nucleotide mutations that lead to the D91A and G128R substitutions, respectively, in the *SOD1* polypeptide (Fig. 1B, Supplementary Table S1).

We introduced these mutations, using CRISPR/Cas9, into a well-characterized control iPSC line (K7-4Lf), obtained earlier from a clinically healthy individual<sup>33</sup> (Supplementary Table S2) and recovered 66 clones for the D91A variant and 124 clones for the G128R variant of which 6 (9.1%) and 4 (3.2%) clones, respectively, were positive for the target mutations. As a result, several clones with different *SOD1* allelic variants were obtained (Fig. 1C). Since we did not find any homozygous variants, we chose clones with *SOD1*<sup>D91A/del105</sup> (iPSC line SOD1-D91A) and *SOD1*<sup>G128R/K129\*</sup> (iPSC line SOD1-G128R) variants for subsequent experiments (Supplementary Fig. S3). Importantly, these clones showed no mutations in five of the most likely predicted off-target sites (Supplementary Fig. S4).

**Generation of iPSC lines modified with genetically encoded biosensors of H<sub>2</sub>O<sub>2</sub> via CRISPR/Cas9-mediated *AAVS1* targeting.** We introduced sequences of two genetically encoded biosensors, Cyto-roGFP2-Orp1, and Mito-roGFP2-Orp1, measuring H<sub>2</sub>O<sub>2</sub> levels in the cytoplasm and mitochondria respectively, in the genome of SOD1-D91A, SOD1-G128R, and the isogenic control line (K7-4Lf) to obtain stable expression. Additionally, we introduced the same sequences in the genome of a patient-specific iPSC line (iALS) previously generated in our lab from a person diagnosed with a hereditary form of ALS with a homozygous D91A mutation in *SOD1*<sup>34</sup>.

The Tet-On system, applied for the biosensors expression, consists of two elements: the biosensor's sequence under the control of the tetracycline-dependent promoter and the specific transactivator (rtTA, reverse tetracycline-controlled transactivator) essential for the controlled expression of the target genes<sup>35</sup>. To deliver these elements in the cell's genome, we used biallelic target insertion in the safe harbor *AAVS1* locus via CRISPR/Cas9 (Fig. 2A). The donor plasmids were either obtained from the vendor or constructed in our laboratory<sup>36,37</sup> (Supplementary Fig. S5). iPSC clones with the target insertions were selected using respective media and tested for the presence of the biosensors' expression in response to doxycycline (tetracycline derivative) addition (Fig. 2B). Selected clones were further examined for target and off-target insertions by PCR (Fig. 2C). Three clones for each cell line were selected for differentiation and analysis (Supplementary Fig. S6).

**Neuronal differentiation of the modified iPSC lines and the biosensor expression in iPSC-derived motor neurons.** We utilized a previously described protocol of highly efficient MN differentiation<sup>38</sup>. All iPSC-derived MNs stained positively for the most common markers: choline acetyltransferase (ChAT), ISL LIM homeobox 1 (ISL1), and motor neuron and pancreas homeobox (MNX1), and expressed mRNA of these proteins (Supplementary Fig. S7). Differentiation efficiency, analyzed on day 20 of differentiation by counting the ISL-positive cells using flow cytometry, showed 89–95% of MNs in the samples (Fig. 3A).

To characterize MNs obtained, we measured the axonal length of the iPSC-derived MNs on day 21 of differentiation. SOD1-D91A (90.7 ± 42.6 μm) and iALS (90.4 ± 41.9 μm) MNs had considerably shorter axonal processes compared to the control K7-4Lf MNs (107.8 ± 45.5 μm). The mean axon length in SOD1-G128R (67 ± 30.6 μm) MNs was even lower, suggesting a highly disturbed function of these cells (Fig. 3B).

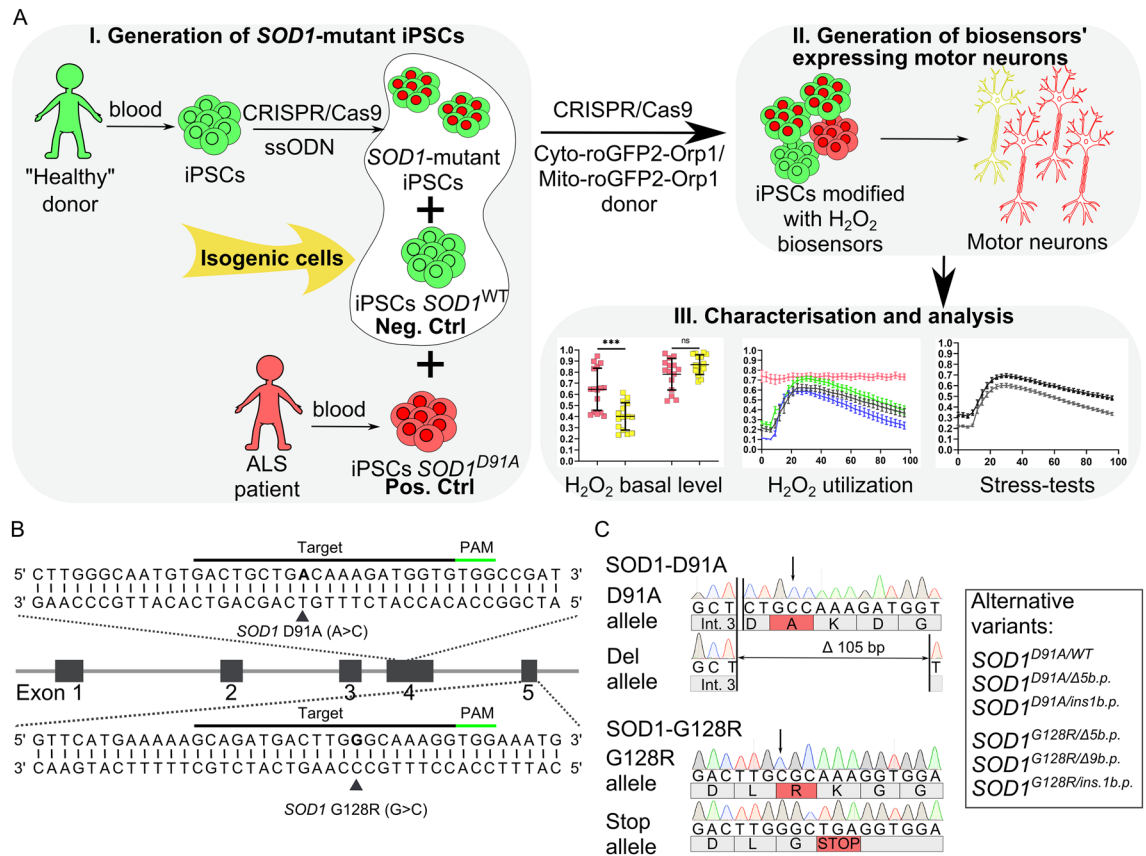


**Figure 1.** Generation of isogenic *SOD1*-mutant iPSC lines. (A) Schematic representation of the experimental design. Induced pluripotent stem cell (iPSC) lines with *SOD1* mutations were generated either from iPSCs of a healthy donor by CRISPR/Cas9-mediated genome editing or obtained from a patient with ALS. The iPSCs from a healthy donor served as an isogenic negative control (Neg. Ctrl); patient-specific iPSCs served as a positive control (Pos. Ctrl). Next, the iPSC lines (control, *SOD1*-mutated, and patient-specific) were modified with biosensors of cytoplasmic (Cyto-roGFP2-Orp1) and mitochondrial (Mito-roGFP2-Orp1) H<sub>2</sub>O<sub>2</sub> by targeted insertion of the biosensors' sequences with CRISPR/Cas9. Then, the modified iPSC lines were differentiated in spinal motor neurons with subsequent analysis of the redox state of the neurons with the biosensors. (B) Schematic of the *SOD1* gene with partial sequences of exons 4 and 5. Protospacers designed for CRISPR/Cas9-mediated double-stranded breaks are underlined with black lines, protospacer adjacent motif (PAM)—with green lines; target mutations are in bold and marked with black triangles. (C) Partial *SOD1* sequences of exons 4 and 5 of the *SOD1*-D91A and *SOD1*-G128R iPSC lines. Int. 3—*intron 3*, substituted nucleotides marked with an arrow, corresponding mutated amino acids are highlighted in red. The box contains a list of clones with alternative *SOD1* variants obtained in the study.

The AAVS1 site is located in the intron of a transcriptionally active gene and was described previously as suitable for stable expression of transgenes<sup>39</sup>. However, we have discovered that the MNs did not always retain a detectable fluorescence level of the biosensor at the terminal stages of differentiation, and this did not depend on a particular cell line (Fig. 3C,D). Analysis of the expression level of rtTA and roGFP2 in the MNs with low intensity of the biosensor signal revealed that the terminally differentiated MNs expressed mRNA of the rtTA at the same level as the corresponding iPSCs from which they were obtained. At the same time, the expression of the biosensor roGFP2 was decreased by two orders, suggesting that the promoter of the biosensor was selectively inhibited (Fig. 3E). We performed differentiation, supplementing the medium regularly with doxycycline from the first day of differentiation to keep the biosensor promoter in an active state. As a result, the biosensor retained high signal intensity in the differentiated MNs as well as mRNA expression on a level comparable to the iPSCs (Fig. 3E). Moreover, the dynamic range (difference between fully oxidized and fully reduced biosensor's state) of the signals generated in the MNs was relatively stable across the lines, suggesting a similar level of the biosensor expression (Supplementary Fig S8).

**Nutrient deprivation affects the mitochondrial level of H<sub>2</sub>O<sub>2</sub> regardless of the genotype.** The basal level of H<sub>2</sub>O<sub>2</sub> reflects stationary redox balance and the general condition of the cell. The H<sub>2</sub>O<sub>2</sub> biosensor allows us to estimate the relative amount of H<sub>2</sub>O<sub>2</sub> molecules in the compartment and determine if it is different from the control. We performed live imaging of the mature MNs (Day 29) at the end of the differentiation protocol to obtain information about their redox state. We did not observe any signs of pathological oxidation in the cytoplasm and mitochondria of the *SOD1*-D91A and iALS MNs. *SOD1*-G128R MNs, however, demonstrated

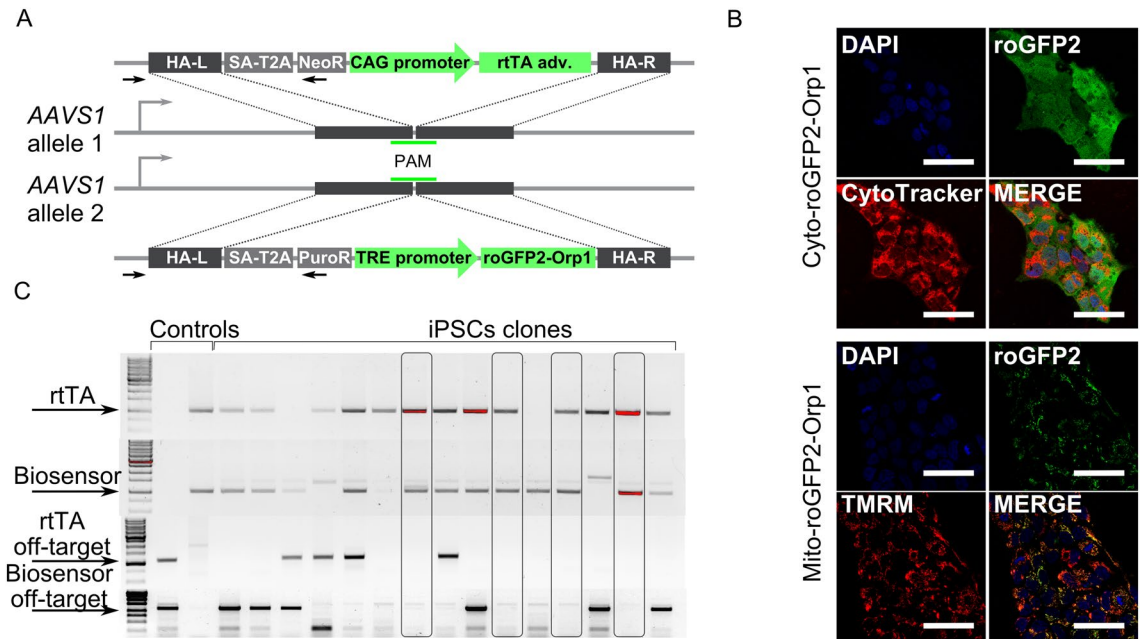


**Figure 2.** Generation of iPSCs expressing the Cyto-roGFP2-Orp1 and Mito-roGFP2-Orp1 biosensors. (A) Schematic of the biosensor and transactivator for doxycycline-controllable expression inserts in the *AAVS1* locus. In one allele, homologous arms (HA-L—left, HA-R—right) flank the splice acceptor site (SA), T2A peptide, neomycin-resistance gene, and reverse tetracycline-controlled transcriptional activator (rtTA) under control of the CAG promoter. In another allele, homologous arms flank the splice acceptor site (SA), T2A peptide, puromycin-resistance gene, and the biosensor's sequence under control of the TRE-promoter. The primers used to detect the target insertions are represented as black arrows. (B) Representative images of live iPSCs expressing the Cyto-roGFP2-Orp1 (top) or Mito-roGFP2-Orp1 (bottom) biosensors 24 h after the addition of 2 mg/ml doxycycline in the medium. Scale bar 50  $\mu$ m. TMRM—tetramethylrhodamine methyl ester perchlorate. (C) Screening of the iPSC clones for the target (two top gels) and off-target (two bottom gels) inserts. The arrows mark target PCR products. The clones positive for the target and negative for the off-target inserts are in frames.

a 2.7 times higher level of the cytoplasmic and five times higher level of the mitochondrial  $H_2O_2$  compared to the control (Fig. 4A). Notably, the cytoplasmic oxidation measured at the stage of immature MNs (Day 20) was similar for all neurons, suggesting that the SOD1-G128R MNs hyper oxidation develops with the maturation of the MNs (Fig. 4B). To correct the observed phenotype, we added a combination of neurotrophic factors (NTFs, See Materials and Methods) to the culture medium during SOD1-G128R MNs maturation (differentiation days 19–29). This resulted in a significant decrease in cytoplasmic  $H_2O_2$  to the normal level. However, it did not affect the mitochondrial level of  $H_2O_2$  (Fig. 4C).

To put additional stress on the MNs, we depleted culturing medium from the majority of the nutrients by removing the B-27 supplement (chemically-defined mixture of antioxidant enzymes, proteins, vitamins, and fatty acids) 24 h before live imaging and measured the cytoplasmic and mitochondrial  $H_2O_2$  levels. We discovered that B-27 deprivation did not influence the cytoplasmic level of  $H_2O_2$  (Fig. 4A,D, Supplementary Fig. S9). However, MNs cultured in the absence of B-27 demonstrated a significant increase in the mitochondrial  $H_2O_2$  level, which was, on average, four times higher than in the cytoplasm of the corresponding neurons. For the SOD1-G128R MNs, the B-27 deprivation resulted in an additional increase in both cytoplasmic and mitochondrial  $H_2O_2$  levels (Fig. 4D, Supplementary Fig. S9).

Interestingly, the  $H_2O_2$  levels in the cytoplasm and mitochondria of mature iALS MNs were lower compared to the control, probably due to the different origin of the iALS cell line (Fig. 4A,D).

**Antioxidants removal from the medium induces  $H_2O_2$  accumulation in the cytoplasm of motor neurons.** Amongst many additives, the neuronal medium contains antioxidants, such as ascorbic acid, vitamin E, vitamin E acetate, superoxide dismutase, catalase, and glutathione, acting against ROS that appear in the medium during in vitro culturing. The removal of the antioxidants from the medium may force MNs to rely on endogenous antioxidant systems for ROS neutralization, making the mutant MNs more vulnerable. We cultured the neurons in the antioxidant-free medium (without ascorbic acid, and using the B-27 supplement without antioxidants) for three days in addition to the differentiation protocol and performed live imaging of the MNs (Day 32, Fig. 5A,B). All MNs showed an increase in the cytoplasmic  $H_2O_2$  level by 1.5–2.5 times. However, only in the SOD1-G128R MNs the mitochondrial level of  $H_2O_2$  increased along with the cytoplasmic level. In addition, SOD1-G128R MNs also demonstrated visible changes in the morphology with the axon attrition and cytoplasmic vacuolization (Fig. 5C). Culturing of SOD1-G128R MNs with the NTFs reduced oxidation of the

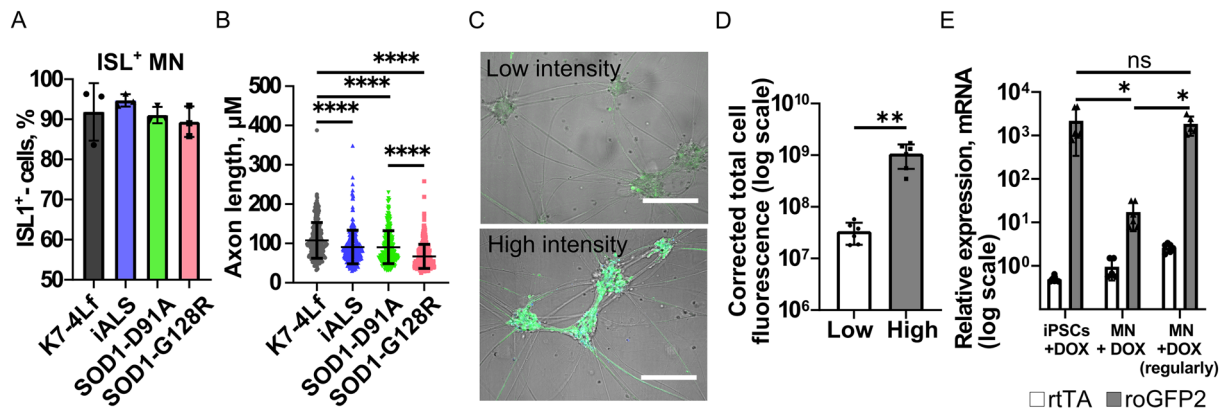


**Figure 3.** Generation of iPSC-derived motor neurons (MNs) expressing the Cyto-roGFP2-Orp1 and Mito-roGFP2-Orp1 biosensors. **(A)** Quantification of flow cytometry analysis of ISL-positive cells was performed on day 20 of the differentiation protocol: K7-4Lf (isogenic control MNs without mutations), iALS (patient-specific MNs with D91A mutation in *SOD1*), SOD1-D91A (isogenic MNs with D91A mutation in *SOD1*), and SOD1-G128R (isogenic MNs with G128R mutation in *SOD1*). Data (N=3 independent differentiations) are the mean  $\pm$  standard deviation (S.D.) **(B)** Axon length quantification (differentiation day 21). Data was collected from three independent differentiations with a total of 257, 270, 409, and 397 cells analyzed for K7-4Lf, iALS, SOD1-D91A, and SOD1-G128R MNs, respectively, and are presented as the mean  $\pm$  S.D. **(C)** Representative images of the MNs with low (top) and high (bottom) intensity signals from Cyto-roGFP2-Orp1. Scale bar 100  $\mu$ m. **(D)** Quantification of the Cyto-roGFP2-Orp1 fluorescence intensity in the MNs with low and high Cyto-roGFP2-Orp1 signal intensity. Data (N=6 independent differentiations) are the mean  $\pm$  S.D. **(E)** RT-qPCR analysis of the tetracycline-controlled transcriptional activator (rtTA) and biosensors (roGFP2) mRNA expression 48 h after 2  $\mu$ g/ml doxycycline addition. iPSCs + DOX—iPSCs expressing biosensor; MN + DOX—MNs supplemented with doxycycline after completion of the differentiation protocol; MN + DOX (regularly)—MNs differentiated with regular doxycycline supplementation. Data (N=6 independent differentiations) are the mean  $\pm$  S.D. \*\*p < 0.01, \*\*\*\*p < 0.0001, one-way ANOVA with post hoc Tukey's tests for **(B)** and **(E)**, Welch t-test for **(D)**.

cytoplasm, but it failed to keep it to the normal level. Moreover, the mitochondrial level of H<sub>2</sub>O<sub>2</sub> was unaffected by addition of the NTFs (Fig. 5D).

**Cyto-roGFP2-Orp1 biosensor, expressed in motor neurons, reflects the kinetics of H<sub>2</sub>O<sub>2</sub> neutralization.** To assess the dynamic response of the MNs expressing Cyto-roGFP2-Orp1 and Mito-roGFP2-Orp1 biosensors to oxidation, we first determined the concentration of H<sub>2</sub>O<sub>2</sub> that did not affect MN viability in the culture. Only treatment with 10  $\mu$ M H<sub>2</sub>O<sub>2</sub> did not significantly affect the viability of the tested MNs (Supplementary Fig. S10), which was consistent with the previously published data<sup>40,41</sup>. Next, we tested whether culturing in the standard neuronal medium distorts the cellular response to the H<sub>2</sub>O<sub>2</sub> and performed a live recording of the Cyto-roGFP2-Orp1-expressing MNs reaction to the addition of 10  $\mu$ M H<sub>2</sub>O<sub>2</sub>. These MNs were either cultured in the standard differentiation medium or starved in the nutrient-deprived medium before the measurement (Fig. 6A). The overall reaction of the cells was similar: MNs expressing Cyto-roGFP2-Orp1 displayed oxidation followed by slow reduction, reflecting the change in the cytoplasmic H<sub>2</sub>O<sub>2</sub> level. However, the reaction of MNs cultured in the nutrient-deprived medium before the experiment was more prominent. We detected a higher delta of the biosensor oxidation and faster reduction compared to the non-starved MNs (Fig. 6B,C). Since components present in the standard medium affected the cellular reaction, we conducted further measurements of the dynamic response on the cells that were starved before the experiment. Using the parameters established earlier, we recorded the reaction of MNs expressing the Mito-roGFP2-Orp1 biosensor to 10  $\mu$ M H<sub>2</sub>O<sub>2</sub> in real-time. We did not detect any response of the Mito-roGFP2-Orp1 biosensor to the exogenous H<sub>2</sub>O<sub>2</sub>. An oxidation value of the biosensor remained constant during imaging, suggesting that the mitochondrial H<sub>2</sub>O<sub>2</sub> level was also stable (Fig. 6D). The addition of H<sub>2</sub>O<sub>2</sub> in higher concentrations (25  $\mu$ M and 50  $\mu$ M) induced mitochondrial oxidation but damaged the neurons. With this finding, we decided not to measure the dynamic response for the Mito-roGFP2-Orp1 sensor (Fig. 6E).

Next, we analyzed how the mutations introduced in *SOD1* affected neuronal reaction to exogenous H<sub>2</sub>O<sub>2</sub>. We did not find any differences in H<sub>2</sub>O<sub>2</sub> utilization in the cytoplasm of Cyto-roGFP2-Orp1-expressing SOD1-D91A, iALS, and control (K7-4Lf) MNs (Fig. 6F–H). Analysis of the SOD1-G128R MNs response to the H<sub>2</sub>O<sub>2</sub> revealed an aberrant reaction. Due to the high initial oxidation of the MNs, cells did not respond to the exogenous H<sub>2</sub>O<sub>2</sub> (Fig. 6F–H). Although culturing of the SOD1-G128R MNs with the NTFs slightly reduced initial oxidation of the cytoplasm, it did not affect the cellular reaction to the H<sub>2</sub>O<sub>2</sub>. The Cyto-roGFP2-Orp1-expressing MNs demonstrated moderate oxidation of the cytoplasm without signs of subsequent reduction (Fig. 6I).

**Motor neurons expressing the Cyto-roGFP2-Orp1 biosensor accumulate H<sub>2</sub>O<sub>2</sub> in the cytoplasm due to glutamate-induced excitotoxicity.** Glutamate excitotoxicity is a known pathological hallmark

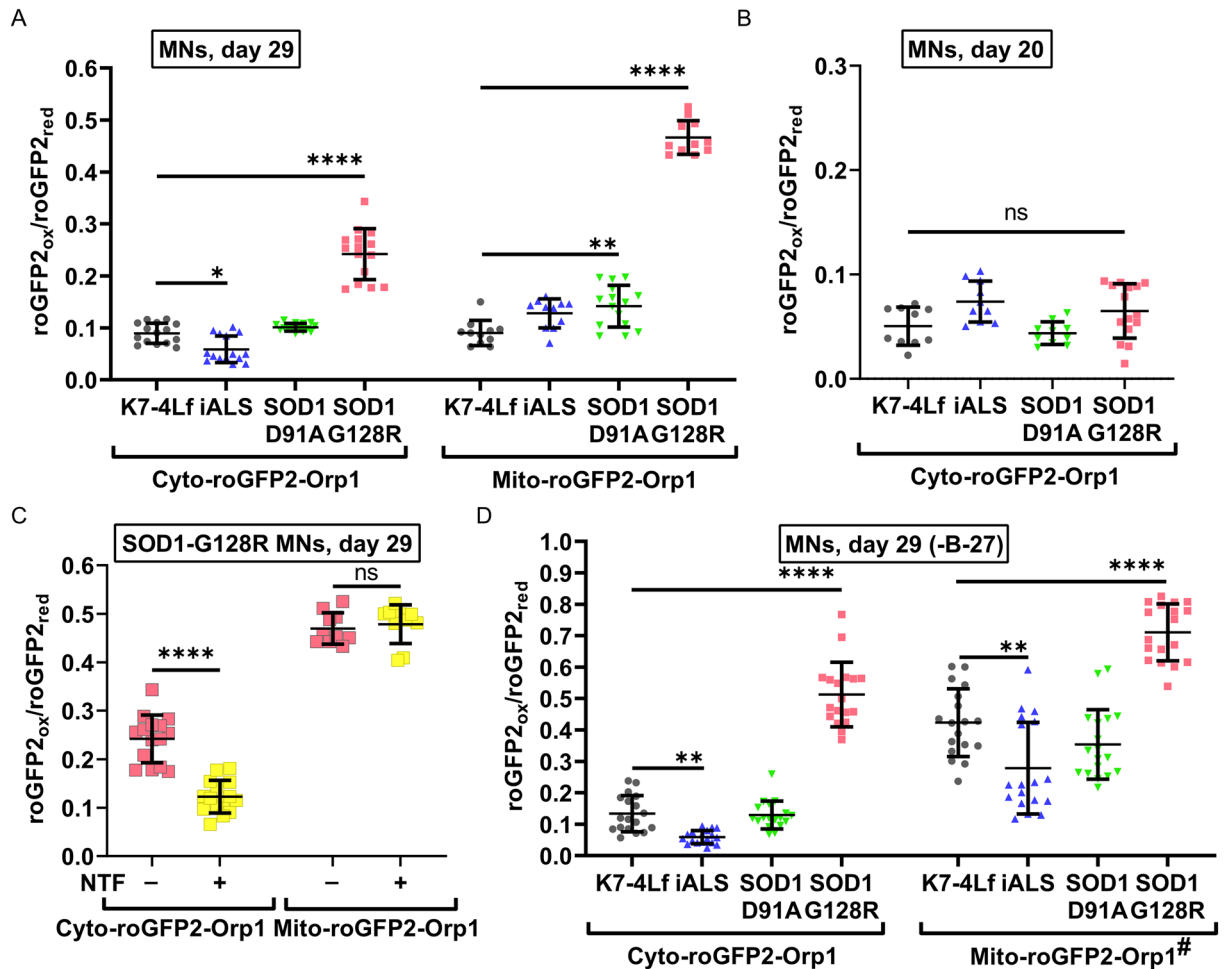


**Figure 4.** Basal levels of  $\text{H}_2\text{O}_2$  in the cytoplasm (Cyto-roGFP2-Orp1) and mitochondria (Mito-roGFP2-Orp1) of the biosensor-expressing motor neurons (MNs) measured at different time points of the differentiation protocol. Values were obtained by analyzing the microscopic images of the respective MNs. **(A)** Day 29 of differentiation. **(B)** Day 20 of differentiation. **(C)** Day 29 of differentiation. SOD1-G128R MNs were cultured with or without neurotrophic factors (NTFs) during maturation. **(D)** Day 29 of differentiation. The standard neuronal medium was replaced by the nutrient-deprived (-B-27) medium 24 h before the measurement. Data ( $N = 10\text{--}15$ , and 18 for B-27 deprived samples, fields of view, collected from MNs, derived from three iPSC lines with the same genotype) are the mean  $\pm$  standard deviation \* $p < 0.05$ , \*\* $p < 0.01$ , \*\*\*\* $p < 0.0001$ , one-way ANOVA with post hoc Dunnett's tests for **(A)**, **(B)**, and **(D)**, Welch t-test for **(C)**. The same datasets of the cytoplasmic and mitochondrial  $\text{H}_2\text{O}_2$  levels in SOD1-G128R (-NTF) were used in **(A)** and **(C)**.

of neurodegeneration<sup>42</sup>. To test whether the Cyto-roGFP2-Orp1 and Mito-roGFP2-Orp1 biosensors can reflect redox imbalance caused by the excitotoxicity, we incubated MNs, expressing these biosensors with monosodium glutamate (20  $\mu\text{M}$ ) and the glutamate reuptake inhibitor (PDC, 100  $\mu\text{M}$ ) for five days and measured the cytoplasmic and mitochondrial  $\text{H}_2\text{O}_2$  levels. Since SOD1-G128R MNs died shortly after the beginning of the experiment due to reduced viability, the measurement was conducted only for K7-4Lf, SOD1-D91A, and iALS MNs. We discovered that the glutamate treatment induced the accumulation of  $\text{H}_2\text{O}_2$  in the cytoplasm regardless of the MN genotype (Fig. 7A). Cytoplasmic oxidation in iALS MNs treated with glutamate was higher compared to the glutamate-treated control MNs. However, we did not find the same for the SOD1-D91A MNs (Fig. 7A), indicating that this effect was not due to the SOD1 mutation. We did not observe the same for the mitochondria, despite the known connection of mitochondrial dysfunction with excitotoxicity (Fig. 7A)<sup>43</sup>. The mitochondrial oxidation in SOD1-D91A MNs in both control and glutamate treated samples was increased (Fig. 7B), although we were unable to determine if the oxidation was a hallmark of the SOD1 mutation or a technical artifact.

Further, we investigated how incubation with monosodium glutamate affected the dynamics of  $\text{H}_2\text{O}_2$  utilization in the cytoplasm of the Cyto-roGFP2-Orp1-expressing MNs. We found that MNs treated with glutamate had a reduced recovery rate after the  $\text{H}_2\text{O}_2$  addition compared to the non-treated sample (Fig. 7C–G).

## Discussion

Nowadays, genetically encoded biosensors are frequently applied to research physiological and pathological processes<sup>44,45</sup>, replacing molecular probes. Indeed, they have provided extensive information about the dynamics of redox balance components, e.g.,  $\text{H}_2\text{O}_2$  or GSH/GSSG ratio, in different cell compartments and tissues<sup>22,46</sup>.

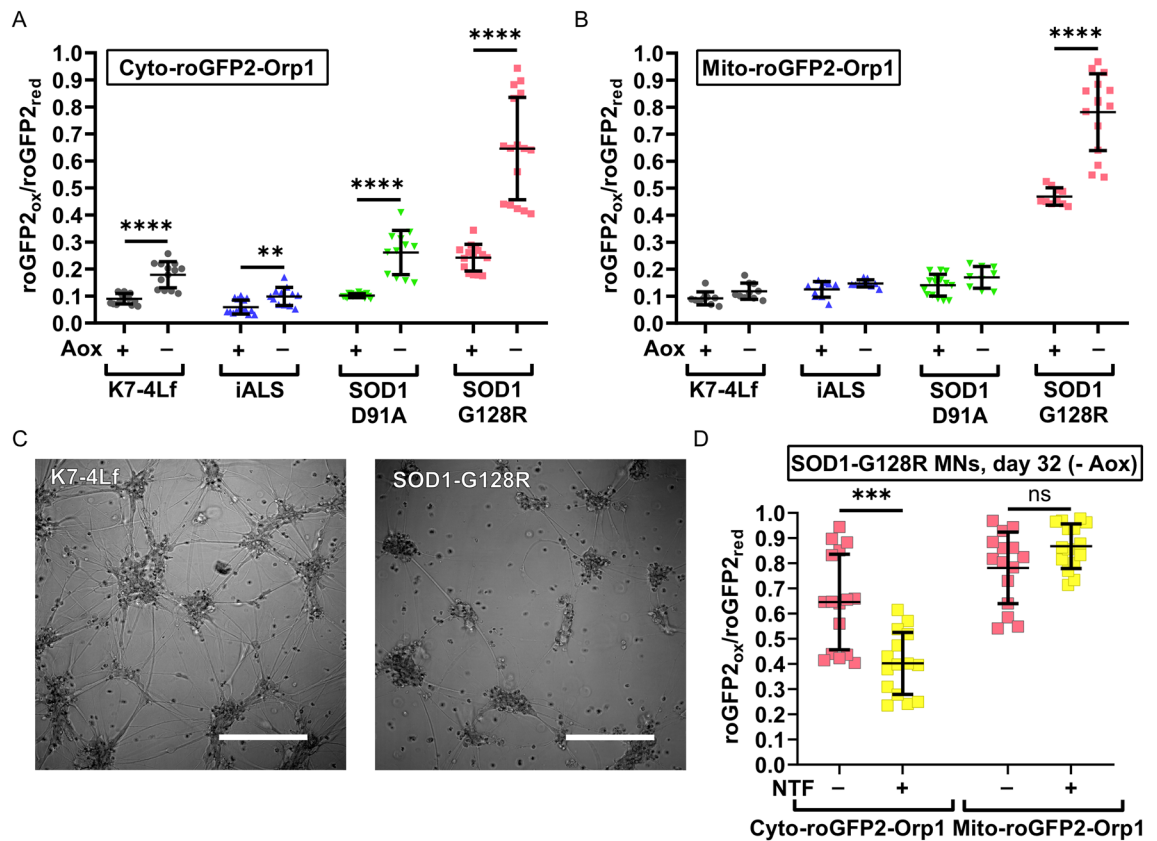


**Figure 5.** Effect of the antioxidant deprivation on the basal  $H_2O_2$  level in the cytoplasm and mitochondria of motor neurons (MNs). Values were obtained by analyzing the microscopic images of the respective MNs. Basal levels of  $H_2O_2$  in the cytoplasm (A) and mitochondria (B) of MNs were measured on the differentiation days 29 (Aox+) and 32 (Aox-). C Representative images of the K7-4Lf and SOD1-G128R MN morphology in the antioxidant-free medium (differentiation day 32, DIC contrast), scale bar 200  $\mu$ m. (D) Basal levels of  $H_2O_2$ , measured on the differentiation day 32 in SOD1-G128R MNs cultured with or without neurotrophic factors (NTFs) in the culture medium during maturation. Data (N = 10–16 fields of view, collected from MNs, derived from three iPSC lines with the same genotype) are the mean  $\pm$  standard deviation. Ns—non significant, \*\* $p < 0.01$ , \*\*\* $p < 0.001$ , \*\*\*\* $p < 0.0001$ , Welch t-test. The same datasets of cytoplasmic and mitochondrial  $H_2O_2$  levels in SOD1-G128R (-NTF) were used in (A–C). The datasets used to present the cytoplasmic and mitochondrial oxidation on the differentiation day 29 (Aox+) for K7-4Lf, iALS, SOD1-D91A, and SOD1-G128R MNs in the panels A and B are the same as in Fig. 4A.

Since the biosensor molecules are delivered inside the cells as plasmids for temporal expression or as viral vectors for sequence integration in the genome, the robustness of biosensors-related studies often relies on the efficiency of delivery and location of transgene integration. Here, we tried to improve the existing approach for biosensor experiments by targeted insertion of the cytoplasmic and mitochondrial  $H_2O_2$  biosensors in combination with their controlled expression (Fig. 1A). This approach allowed us to obtain iPSC lines, stably expressing the biosensors, and avoid potential undesirable effects of random integration (Fig. 2). For the first time, to our knowledge, we showed that the biosensor expressing in such a system is a reliable method to study MNs in vitro, as the intensity of the signal generated from a single copy of the biosensor and the dynamic range of that signal, are sufficient for routine imaging (Supplementary Fig. S8). However, we found that the *AAVS1* locus does not support the stable expression of the integrated biosensors in MNs despite its “safe harbor” status, probably, due to chromatin remodeling occurring during differentiation<sup>47</sup>. Although constant activation of the biosensor promoter during differentiation, applied here, prevented it from silencing, this in itself emphasizes the necessity to discover new safe harbors in the human genome (Fig. 3C–E).

The measurements, conducted in MNs with Cyto-roGFP2-Orp1 and Mito-roGFP2-Orp1 biosensors, revealed that the basal level of cytoplasmic and mitochondrial oxidation is dynamic and serves as an indicator of cellular distress. Nutrient deprivation, known to induce moderate stress, activates autophagy through the ROS signaling<sup>48–50</sup>. In our data, MNs deprived of nutrients demonstrated additional oxidation of the mitochondria (Fig. 4), which was in line with the previously published data<sup>48</sup>. Additionally, a stable cytoplasmic level of  $H_2O_2$  in this condition also suggests that this is a part of a natural response. Interestingly, despite the stability of the cytoplasmic  $H_2O_2$  level in the nutrient-deprived MNs, the reaction of the cells to exogenous  $H_2O_2$  was more prominent. Specifically, a higher amplitude of oxidation and faster recovery were recorded (Fig. 6A–C), implying

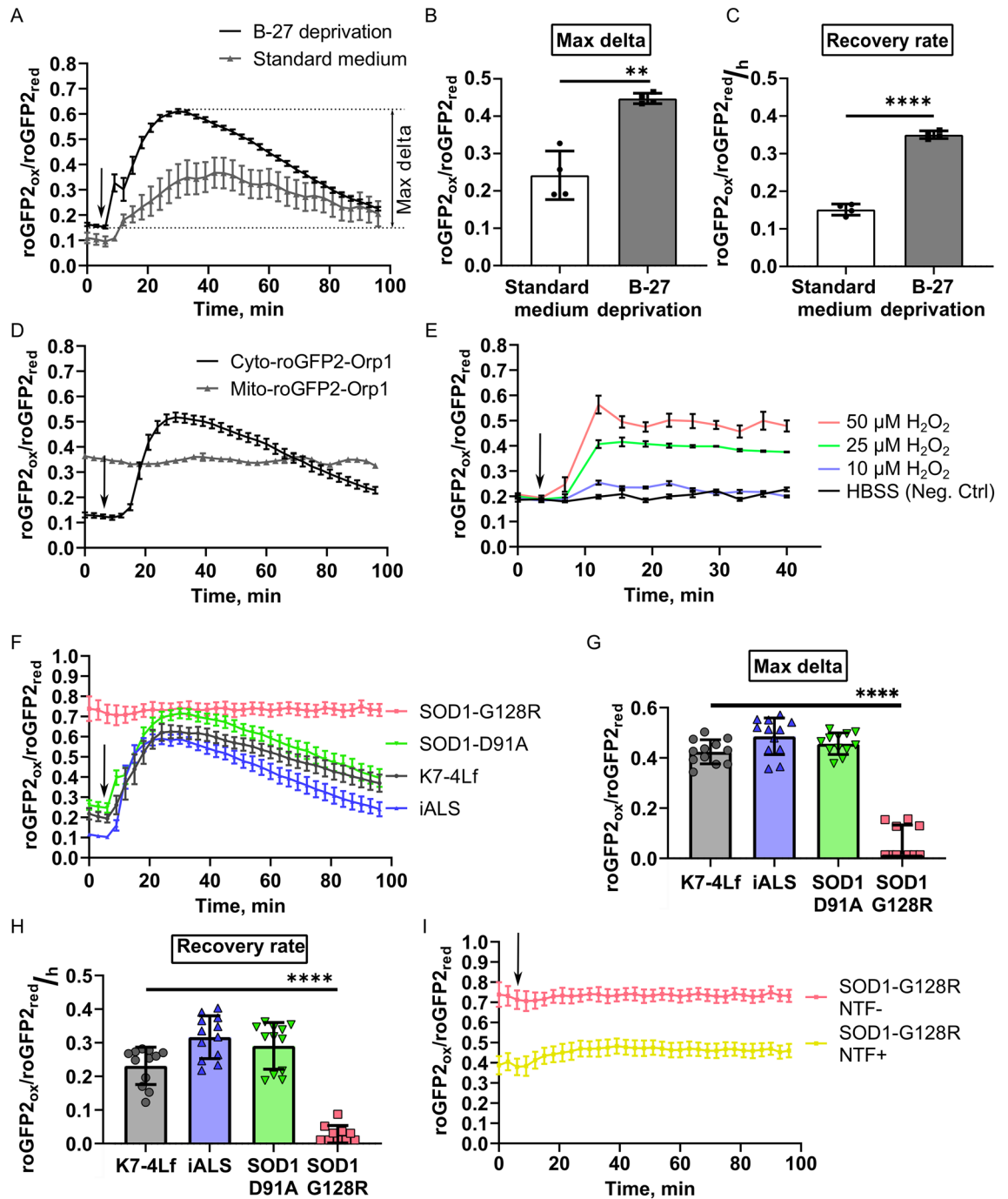


**Figure 6.** Kinetics of  $\text{H}_2\text{O}_2$  utilization in live iPSC-derived motor neurons (MNs). Values were obtained by analyzing the microscopic images of the respective MNs. (A) Response of the MNs, cultured in the standard or nutrient-deprived (without B-27) medium to addition of 10  $\mu\text{M}$   $\text{H}_2\text{O}_2$ . Data (N = 4 fields of view) are the mean  $\pm$  standard error of the mean (S.E.M.). Max delta (difference between the maximum and initial level of oxidation, defined in panel A) of the cytoplasm oxidation (B) and recovery rate (C) of the MNs, expressing Cyto-roGFP2-Orp1, after  $\text{H}_2\text{O}_2$  addition. Data (N = 4 fields of view) are the mean  $\pm$  standard deviation (S.D.). (D) Response of the MNs, expressing Cyto-roGFP2-Orp1 or Mito-roGFP2-Orp1, to addition of 10  $\mu\text{M}$   $\text{H}_2\text{O}_2$ . Data (N = 4 fields of view) are the mean  $\pm$  S.D. (E) Response of the MNs, expressing Mito-roGFP2-Orp1, to the different  $\text{H}_2\text{O}_2$  concentrations. Data (N = 3 fields of view) are the mean  $\pm$  S.D. (F) Response of the K7-4Lf, iALS, SOD1-D91A, and SOD1-G128R MNs, expressing Cyto-roGFP2-Orp1 to addition of 10  $\mu\text{M}$   $\text{H}_2\text{O}_2$ . Data (N = 12 fields of view, collected from MNs, derived from three iPSC lines with the same genotype) are the mean  $\pm$  S.E.M. Max delta of the cytoplasm oxidation (G) and recovery rate (H) of the K7-4Lf, iALS, SOD1-D91A, and SOD1-G128R MNs, expressing Cyto-roGFP2-Orp1 after 10  $\mu\text{M}$   $\text{H}_2\text{O}_2$  addition. Negative values in the SOD1-G128R MNs were set to 0 on the graphs. Data (N = 12 fields of view, collected from MNs, derived from three iPSC lines with the same genotype) are the mean  $\pm$  S.D. (I) Response of the SOD1-G128R MNs, expressing Cyto-roGFP2-Orp1 cultured in the standard medium (NTF-) or medium supplemented with neurotrophic factors (NTF+) to 10  $\mu\text{M}$   $\text{H}_2\text{O}_2$ . Data (N = 4 fields of view) are the mean  $\pm$  S.E.M. The moment of the  $\text{H}_2\text{O}_2$  addition is marked by an arrow. \*\* $p < 0.01$ , \*\*\*\* $p < 0.0001$ . Welch t-test for (B), and (C), one-way ANOVA with post hoc Dunnett's tests for (G) and (H). The same dataset was used in Figs. 7E/I to represent the SOD1-G128R (-NTF) reaction to  $\text{H}_2\text{O}_2$ .



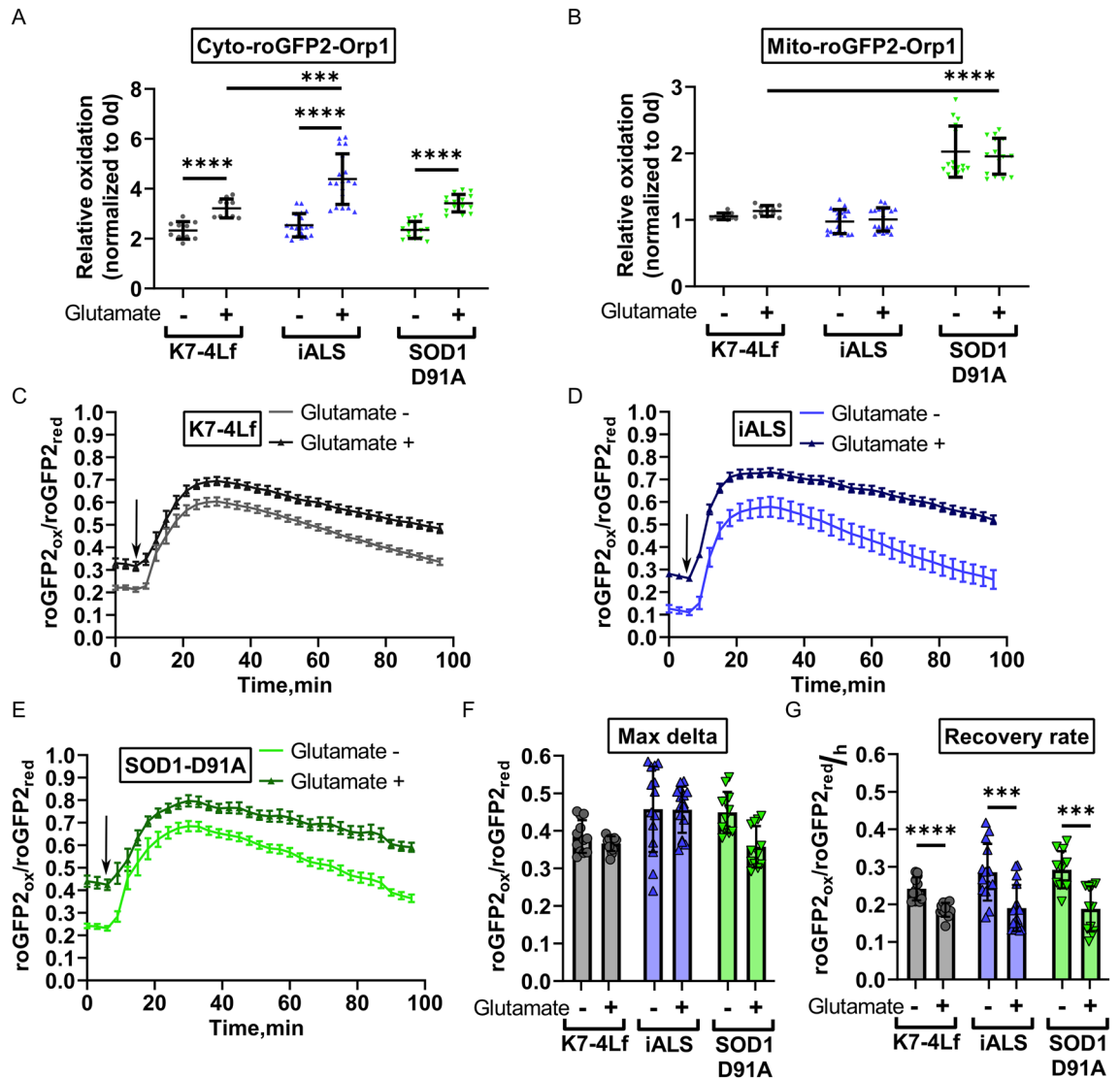


**Figure 7.** The reaction of iPSC-derived motor neurons (MNs) to excitotoxicity. Values were obtained by analyzing the microscopic images of the respective MNs. Basal level of  $\text{H}_2\text{O}_2$  in the cytoplasm (A) and mitochondria (B) of MNs after 5-days incubation with monosodium glutamate ( $20 \mu\text{M}$ ) + PDC ( $100 \mu\text{M}$ ). Data ( $N = 10\text{--}15$  fields of view, collected from MNs, derived from three iPSC lines with the same genotype) are normalized to the basal  $\text{H}_2\text{O}_2$  level measured before the addition of glutamate and presented as the mean  $\pm$  standard deviation (S.D.). The response of K7-4Lf (C), iALS (D), and SOD1-D91A (E) MNs to addition of  $10 \mu\text{M}$   $\text{H}_2\text{O}_2$  (marked by an arrow). The reaction of MNs cultured with glutamate is depicted in the darker colors. Data ( $N = 12$  fields of view, collected from MNs, derived from three iPSC lines with the same genotype) are the mean  $\pm$  standard error of the mean (S.E.M.) Max delta (difference between maximum and initial level of oxidation) of the cytoplasm oxidation (F) and recovery rate (G) of the MNs expressing Cyto-roGFP2-Orp1 after addition of  $10 \mu\text{M}$   $\text{H}_2\text{O}_2$ . Data ( $N = 12$  fields of view, collected from MNs, derived from three iPSC lines with the same genotype) are the mean  $\pm$  S.D. \* $p < 0.05$ , \*\*\* $p < 0.001$ , \*\*\*\* $p < 0.0001$ , Welch t-test for paired comparisons in (A, B, F, G), one-way ANOVA with post hoc Dunnett's tests for comparisons between MNs, treated with glutamate in (A) and (B).

that in these moderate stress conditions, the buffering capacity of the cytoplasm is lower, but the antioxidant system is in the mobilized, more active state<sup>51</sup>.

Differences in cytoplasmic and mitochondrial reactions to the exogenous  $\text{H}_2\text{O}_2$  reflect relative independence of the mitochondrial and cytoplasmic antioxidant systems (Fig. 6D–E). The absence of significant changes in the signal of the Mito-roGFP2-Orp1 sensor and the presence of a normal reaction of the Cyto-roGFP2-Orp1 sensor in response to  $10 \mu\text{M}$   $\text{H}_2\text{O}_2$  suggests that the cytoplasmic antioxidant system neutralizes most exogenous  $\text{H}_2\text{O}_2$  molecules. The reaction that only appears in response to a lethal amount of  $\text{H}_2\text{O}_2$  suggests that exceeding hydrogen peroxide level in the cytoplasm above the value that it can quickly neutralize leads to a transfer of  $\text{H}_2\text{O}_2$  molecules into mitochondria and apoptosis induction<sup>52</sup>.

To test if the developed platform can reflect pathological oxidation in MNs caused by a genetic mutation, we generated isogenic cell lines with *SOD1* mutations of, presumably, different severity: D91A and G128R<sup>31,32</sup>. Since no homozygous variants have been found, we selected the lines that have one allele with the target mutation and the other with large deletion (SOD1-D91A) or premature termination codon (SOD1-G128R) to maximize potential damage and make the pathological phenotype more perceptible (Fig. 1B,C). While the neurons generated from iPSC lines with a D91A mutation were not different from the control, MNs derived from the SOD1-G128R iPSCs demonstrated higher levels of oxidation in both the cytoplasm and mitochondria, which only increased in stress conditions, such as nutrient or antioxidant deprivation (Figs. 4, 5, 6). Through live imaging of the neurons in the different stages of differentiation, we were able to detect that described pathological features only appear in the latest stages of differentiation (Fig. 4B), which is consistent with the fact that ALS does not manifest until a certain age<sup>53</sup>. Using the separate measurement of H<sub>2</sub>O<sub>2</sub> in different compartments, we were able to detect that mitochondrial oxidation in mature SOD1-G128R MNs was more pronounced than that of the cytoplasm (Figs. 4A, 5A,B), suggesting that accumulation of H<sub>2</sub>O<sub>2</sub> in mitochondria precedes its accumulation in the cytoplasm. Together with the slower axon growth (Fig. 3B), this could be a sign of mitochondrial dysfunction that has been linked to neurodegeneration before<sup>1,54</sup>. Moreover, the inability of neurotrophic factors to correct this phenotype indicates the severity and irreversibility of the cellular condition observed at this point (Figs. 4C, 5D).

Glutamate excitotoxicity is one of the major mechanisms of ALS development, in which excessive activation of the glutamate receptors leads to mitochondrial dysfunction and apoptosis<sup>42,52</sup>. It is known that this process is accompanied by increased ROS production, which connects it with oxidative stress<sup>55</sup>. In our study, we, for the first time, observed in live MNs how glutamate-induced excitotoxicity affected oxidation in the neuronal compartments. Glutamate-treated neurons demonstrated accumulation of H<sub>2</sub>O<sub>2</sub> in the cytoplasm and a slower recovery rate after H<sub>2</sub>O<sub>2</sub> addition (Fig. 7). However, no differences between the D91A mutant and control MNs were observed, suggesting that the power of stress applied or the degree of MN maturation was insufficient for the pathological phenotype to manifest, meaning that further optimization of the study parameters is required.

In conclusion, our work presents a new approach for the application of cell-based disease models for research that can be used to generate other similar models. We expect this approach to be expanded to include other disease-associated mutations or the biosensors of other cellular processes. There are, however, still elements that require further optimization, such as research for the new safe-harbor loci that sustain transgene expression. Moreover, the culture conditions applied for the study must be considered since modern cell culture systems are highly protective and can hinder the results of the measurements. We also look forward to the application of automated cell imaging, allowing continuous measurement during cell differentiation and maturation, which could also be beneficial for more complex research and screening for future therapeutics.

## Methods

**iPSC cell culture.** iPSCs were maintained on the layer of mitotically inactivated mouse embryonic fibroblasts in KnockOut DMEM (Gibco) with 15% knockout serum replacement (Gibco), 0.1 mM non-essential amino acids (Gibco), penicillin/streptomycin (Lonza), 1 mM GlutaMAX-I, and 10 ng/mL bFGF at 37 °C and 5% CO<sub>2</sub>. iPSCs were dissociated with TrypLE (Gibco) and split at 1:10 twice a week in the iPSC medium supplemented with 10 ng/ml Y-27632. Original iPSC lines were derived from the patient (iALS) with a diagnosed hereditary form of ALS<sup>37</sup> and a healthy individual (K7-4Lf) who had no associations with any genetic disease<sup>33</sup> (Supplementary Table S2). The use of the iPSC lines, generated from the patients' materials, in the study has been approved by the Research Ethics Committee of FSBI Federal Neurosurgical Center (Novosibirsk, Russia), protocol number 1 14/03/2017.

**Generation of iPSC lines with the c.272A>C (D91A) and c.382G>C (G128R) substitutions in *SOD1*.** The guide RNAs (gRNAs) targeting sequences in exons 4 and 5 of the *SOD1* gene and the *AAVSI* locus were designed using the web-based tool <http://crispr.mit.edu><sup>56</sup>. The Alt-R<sup>+</sup> crisperRNA and tracrRNA were obtained from IDT (Integrated DNA technologies), and Cas9 protein was expressed in *E. coli* and purified according to the previously published protocol<sup>57</sup>. The CRISPR/Cas9 ribonucleoprotein (RNP) complexes were assembled according to the manufacturer's instructions on the day of transfection. For the introduction of the c.272A>C and c.382G>C mutations we used appropriate RNP (20 pmol tracrRNA + 20 pmol crisperRNA (SOD1-4/SOD1-5) + 20 pmol Cas9) complexes mixed with 100 pmol of D91A ssODN (single-stranded oligodeoxynucleotide) or G128R ssODN donor. The cells were passed 24 h before the transfection in the iPSC medium supplemented with Y-27632 (10 ng/ml). Transfection was performed using Neon Transfection System 10 µl Kit (Invitrogen) according to the manufacturer's instructions. The cells were seeded on feeder-coated 4 cm<sup>2</sup> dishes in the iPSC medium supplemented with Y-27632 (10 ng/ml). The next day, the cells were dissociated with TrypLE, strained through the cell strainer, and subcloned on 96-well plates for propagation and analysis. Genomic DNA of the survived clones was obtained and analyzed for the presence of the target mutations.

To detect the c.272A>C mutation, we designed primers for tetra-primer ARMS (amplification-refractory mutation system) PCR screening using <http://primer1.soton.ac.uk/primer1.html><sup>58</sup> and performed touchdown 3-step PCR with annealing at 68–64 °C for 9 cycles, then at 64 °C for 21 cycles. The PCR products were analyzed in 2% agarose gel. Clones positive for the mutant allele were further examined by Sanger sequencing. To detect the c.382G>C mutation, we designed a pair of primers that amplify the target locus of the *SOD1* gene and two fluorescent probes targeting either wild-type or mutant sequences. Using LightCycler 480 (Roche), we analyzed the clones and selected those who had strong signals from the mutant-targeted probe. The target mutation was further confirmed by Sanger sequencing. Potential off-target CRISPR/Cas9 sites were determined using the Benchling algorithm (<https://www.benchling.com/>), and the top 5 hits were then investigated in the obtained cell lines by Sanger sequencing. Clones used in the experiments were characterized according to the Human

Pluripotent Stem Cell Registry standards with the protocols described previously<sup>34</sup>. All oligonucleotides/primers used in the study are listed in the Supplementary Table S1.

**Generation of iPSC lines with target AAVS1 inserts.** To insert Cyto-roGFP2-Orp1, Mito-roGFP2-Orp1 and transactivator in AAVS1, we used AAVS1 RNP (100 pmol tracrRNA + 100 pmol AAVS1 crRNA + 100 pmol Cas9) mixed with 5 µg of donor plasmids mix, containing equimolar amounts of transactivator donor (pAAVS1-Neo-M2rtTA, Addgene # 60843) + pCyto-roGFP2-Orp1-donor or pMito-roGFP2-Orp1-donor. The transfection was performed using Neon Transfection System 100 µl Kit according to instructions. The cells were then seeded on feeder-coated 10 cm<sup>2</sup> dishes in the iPSC medium supplemented with Y-27632 (10 ng/ml) and maintained before the selection until small colonies formed. We supplemented the iPSC medium with puromycin dihydrochloride for 3 days to select subclones with the target inserts. Then we replaced the antibiotic with neomycin sulfate and incubated the cells for 4–5 more days. Antibiotic concentrations were determined for each cell line before the experiment. At the end of the selection, we added doxycycline hyclate (2 µg/ml) and examined the remained clones for the presence of fluorescent signal from the biosensors' roGFP2 using the Nikon Eclipse Ti2-E microscope. The clones positive for roGFP2 expression that survived double antibiotic selection were manually harvested into separate dishes for maintenance and analysis. Genomic DNA extracted from these iPSC clones was analyzed for the presence of the target and off-target inserts of the donor plasmids using PCR (Supplementary Table S1).

**Co-localization of the roGFP2 fluorescent signal with the cytoplasm and mitochondria.** The cells were seeded on Matrigel-coated cell imaging coverglasses in the media, supplemented with doxycycline hyclate (2 µg/ml). On the day of imaging, the cells were incubated in HBSS + Ca<sup>2+</sup>, Mg<sup>2+</sup>, supplemented with cell-permeant nuclear counterstain (NucBlue™ Live ReadyProbes™ Reagent, 2 drops/ml, Thermo Fisher Scientific) and 250 nM tetramethylrhodamine, methyl ester, perchlorate (TMRM, Thermo Fisher Scientific) for mitochondrial staining, or 1 µM CellTracker™ Red CMTPX Dye (Thermo Fisher Scientific) for cytoplasmic staining, for 30 min. Then, cells were washed with HBSS + Ca<sup>2+</sup>, Mg<sup>2+</sup> and immediately visualized. Micrographs were captured using the LSM-780 (Zeiss) microscope and ZEN black software.

**Immunocytochemistry.** The cells were fixed in 4% formaldehyde solution for 10 min at room temperature (RT), permeabilized with 0.5% Triton X-100 for 30 min at RT, and then incubated with blocking buffer (1% bovine serum albumin (BSA) in PBS) for 30 min at RT. After, the cells were incubated with specific primary antibodies overnight at 4 °C. Next, the appropriate secondary antibodies were added for 1.5–2 h incubation at RT. All antibodies were diluted in blocking buffer, and the cell nuclei were visualized with DAPI (1 µg/ml solution in PBS). The antibodies and their dilution ratios are listed in Supplementary Table S11. Micrographs were captured using either Nikon eclipse Ti-E microscope (Nikon) and NIS Elements software or the LSM-780 (Zeiss) microscope and ZEN black software.

**Motor neuron differentiation and maintenance.** The iPSCs were seeded on Matrigel-coated dishes in E8 (Gibco) medium and maintained in feeder-free conditions for at least 2 passages prior to differentiation. MN differentiation was performed according to the previously published protocol<sup>38</sup>. For neural patterning, the E8 medium was changed to neuronal differentiation medium (NDM): F12/DMEM:Neurobasal—50:50, 0.5 × N2 supplement, 0.5 × B-27 supplement, 2 mM GlutaMAX, and 0.1 mM ascorbic acid. For the first six days NDM was supplemented with 2 µM CHIR99021 (StemRD), 2 µM SB431242 (Selleckchem), and 2 µM DMH1 (Tocris). Following this, neuroepithelial cells were dissociated 1:6 with Accutase (Gibco) and maintained for six days in NDM supplemented with CHIR99021, SB431242, DMH1, 0.5 µM Puromorphamin (Stemgent), and 0.1 µM retinoic acid (Sigma). Then, the MN progenitors were dissociated with Accutase and cultured in suspension on agarose-coated (non-adherent) dishes in NDM, supplemented with 0.1 µM Puromorphamin and 0.5 µM retinoic acid for 6 days. For maturation, cells were dissociated with Accutase to a single-cell suspension, strained through the 70 µm cell strainer, and seeded in NDM, supplemented with 0.1 µM Puromorphamin, 0.5 µM retinoic acid, and 0.15 µM Compound E (EMDMillipore). Depending on the experiment, MNs were seeded in different settings: for flow cytometry and mRNA expression analysis, we seeded 1.5 × 10<sup>5</sup> cells/cm<sup>2</sup> on Matrigel-coated 60 mm Petri dishes; for immunocytochemistry—5 × 10<sup>4</sup> cells/cm<sup>2</sup>—on Matrigel-coated cell imaging coverglasses (Eppendorf); for axon measurement—1.5 × 10<sup>4</sup> cells/cm<sup>2</sup>—on Matrigel-coated cell imaging coverglasses; for biosensors live imaging—inside Matrigel layer (see “Supplementary methods”, Supplementary Fig. S12). After each dissociation, cells were transferred to Y-27632-supplemented (10 ng/ml) medium, which was replaced daily. The cells were also supplemented with doxycycline (2 µg/ml) every other day during the differentiation unless otherwise indicated.

For starvation (B-27 deprivation) induction, standard NDM was replaced with nutrient-deprived medium (F12/DMEM:Neurobasal—50:50, 1 × N2 Supplement, 2 µg/ml doxycycline hyclate). For the antioxidant-deprivation assay and excitotoxicity induction assay, MNs were incubated in antioxidant-free medium (F/D:Neurobasal—50:50, 0.5 × N2 supplement, 0.5 × B-27 supplement without antioxidants, 2 µg/ml doxycycline hyclate, 0.5 µM retinoic acid, and 0.15 µM Compound E). For studying the neurotrophic factor effect in MN oxidation, cells were cultured in the respective medium supplemented with IGF1 (PeproTech, 10 ng/ml), CNTF (PeproTech, 10 ng/ml), and BDNF (PeproTech, 10 ng/ml).

**Reverse-transcription quantitative PCR (RT-qPCR).** 1 µg of total RNA extracted with Trizol reagent (Invitrogen) was used for reverse transcription with M-MuLV-RH reverse transcriptase (Biolabmix) and random hexamer primer (Invitrogen) and diluted 1:10 in MilliQ H<sub>2</sub>O. qPCR analysis was performed using the

LightCycler 480 (Roche). Gene expression of iPSC markers in the *SOD1* mutant iPSCs was normalized to the *B2M* housekeeping gene and compared to the original iPSC line using the  $\Delta\Delta C_t$ -method. *ISL1*, *CHAT*, and *MNX1* genes expression in MNs was normalized to the mean of the *GAPDH*, *HPRT1*, and *RPL13* housekeeping genes and compared to that of the iPSC using the  $\Delta\Delta C_t$ -method. The roGFP2 and rtTA transgenes expression in MNs and iPSCs was normalized to the mean of *GAPDH*, *HPRT1*, and *RPL13* housekeeping genes and compared to the expression in MNs that were not treated with doxycycline during differentiation. The primers used are listed in Supplementary Table S2.

**Flow cytometry analysis.** The cells were dissociated with Accutase on day 20 of the differentiation protocol, resuspended in cold PBS, and centrifuged at 400g for 5 min (the same settings were used for all subsequent centrifugation steps). The pellet was resuspended in 1 ml cold 4% formaldehyde solution and incubated on ice for 10–15 min. Next, we added 1 ml cold PBS, centrifuged the cells, discarded supernatant, resuspended the pellet in 1 ml ice-cold 100% methanol, and incubated it for 10–15 min on ice. Then, the pellet was washed twice with flow cytometry staining buffer (1% BSA, 0.2  $\mu$ M EDTA, in PBS) and resuspended in it to  $1 \times 10^6$  cells/ml concentration. 100  $\mu$ l of the cell suspension ( $1 \times 10^6$  cells/ml) was incubated with anti-ISL primary antibodies overnight at 4 °C. The cells were washed with flow cytometry staining buffer, incubated with the secondary antibodies for 30 min at RT, and analyzed using FACSAria (BD Biosciences). Unlabeled cells and isotype-labeled cells were used as controls.

**Fluorescence intensity measurement.** MN images (four for each sample) were obtained using the Zeiss LSM-780 confocal laser scanning microscope (Pan-Apochromat 20 $\times$  objective) adjusted for visualization of a green dye (excitation—488 nm; emission collection at 500–530 nm). Mean intensity of the fluorescence on each image was measured using the ImageJ software and corrected total cell fluorescence (CTCF) was calculated with the formula:  $CTCF = \text{Integrated Density} - (\text{Area occupied by cells} \times \text{Mean fluorescence of background readings})$ .

**Axon measurement.** Immature MNs were seeded on the cell imaging coverglasses and grown for two days in a medium supplemented with a neurotrophic factor (NTF) cocktail: IGF1 (PeproTech, 10 ng/ml), CNTF (PeproTech, 10 ng/ml), and BDNF (PeproTech, 10 ng/ml). Doxycycline (2  $\mu$ g/ml) was added to induce the roGFP2 expression. Images were obtained with the Nikon Eclipse Ti-2E microscope (20 $\times$  objective, FITC channel). Using ImageJ, we manually measured the length of the longest processes (axons) of free-lying neurons with visible ends. Only axons with a length more than twice the size of the neurons' bodies were considered for the analysis. If the neuron had two long processes, the longest one was considered for the measurement. The mean length of the axons was calculated based on the data obtained from the differentiation of three separate iPSC clones for each genotype.

**Image acquisition.** The general procedures for the image acquisition and data analysis, including samples and solution preparations, microscopy settings, biosensors' calibration, basal  $H_2O_2$  measurement,  $H_2O_2$  utilization analysis, and data normalization, are described in the "Supplementary methods".

**XTT viability assay.** The viability of the MNs was assessed 3 h after the addition of  $H_2O_2$  in different concentrations (10  $\mu$ M, 25  $\mu$ M, 50  $\mu$ M, and 100  $\mu$ M) by an XTT test with 2,3-bis-(2-methoxy-4-nitro-5-sulphophenyl)-2H-tetrazolium-5-carboxanilide (Roche), according to the manufacturer's instructions at 20 h after the reagents were added. Cells were seeded on Matrigel-covered 96-well plates ( $1.6 \times 10^4$  cells/well). Before adding  $H_2O_2$ , we replaced the neuronal medium with HBSS +  $Ca^{2+}$  +  $Mg^{2+}$ . For each  $H_2O_2$  concentration, the experiments were carried out in three replicates. The viability data were normalized to the values obtained in the control well, treated with PBS and analyzed by Welch t-test.

**Excitotoxicity induction assay.** MNs were incubated in the neuronal maintenance medium supplemented with 20  $\mu$ M monosodium glutamate (Sigma-Aldrich) and 100  $\mu$ M L-trans-pyrrolidine-2,4-dicarboxylic acid (PDC, Sigma-Aldrich) for 5 days, changing the medium every other day. After 5 days of incubation, we obtained images of the treated MNs and non-treated control MNs. The data obtained at the end of the experiment were normalized to the starting oxidation values, measured before the glutamate addition, to describe the changes that emerged during the experiment.

**Statistics.** Graphs and statistical analyses were performed in GraphPad Prism, version 9.2.0 (<https://www.graphpad.com/scientific-software/prism/>). Statistical analyses were performed using Welch t-test for single-pair comparisons or one-way ANOVA with post hoc Tukey's or Dunnett's tests for multiple comparisons, where applicable.

### Data availability

The datasets used and/or analyzed during the current study are available from the corresponding authors on reasonable request.

Received: 4 November 2021; Accepted: 5 May 2022

Published online: 27 May 2022

## References

- Dias, V., Junn, E. & Mouradian, M. M. The role of oxidative stress in Parkinson's disease. *J. Parkinsons. Dis.* **3**, 461–491 (2013).
- Barber, S. C. & Shaw, P. J. Oxidative stress in ALS: Key role in motor neuron injury and therapeutic target. *Free Radic. Biol. Med.* **48**, 629–641 (2010).
- Chinta, S. J. & Andersen, J. K. Redox imbalance in Parkinson's disease. *Biochim. Biophys. Acta Gen. Subj.* **1780**, 1362–1367 (2008).
- Esposito, S. *et al.* Redox-sensitive GFP to monitor oxidative stress in neurodegenerative diseases. *Rev. Neurosci.* **28**, 133–144 (2017).
- Malkus, K. A., Tsika, E. & Ischiropoulos, H. Oxidative modifications, mitochondrial dysfunction, and impaired protein degradation in Parkinson's disease: How neurons are lost in the Bermuda triangle. *Mol. Neurodegener.* **4**, (2009).
- Machiela, E. *et al.* The interaction of aging and cellular stress contributes to pathogenesis in mouse and human huntington disease neurons. *Front. Aging Neurosci.* **12**, 524369 (2020).
- Ustyantseva, E. I., Medvedev, S. P. & Zakian, S. M. Studying ALS: Current approaches, effect on potential treatment strategy. *Adv. Exp. Med. Biol.* **1241**, 195–217 (2020).
- Rosen, R. D. *et al.* Mutations in Cu/Zn superoxide dismutase gene are associated with familial amyotrophic lateral sclerosis. *Nature* **362**, 59–62 (1993).
- Chen, H., Kankel, M. W., Su, S. C., Han, S. W. S. & Ofengeim, D. Exploring the genetics and non-cell autonomous mechanisms underlying ALS/FTLD. *Cell Death Differ.* **25**, 646–660 (2018).
- Zhang, K. *et al.* The C9orf72 repeat expansion disrupts nucleocytoplasmic transport. *Nature* **525**, 56–61 (2015).
- Bilicer, B. *et al.* Mutant induced pluripotent stem cell lines recapitulate aspects of TDP-43 proteinopathies and reveal cell-specific vulnerability. *Proc. Natl. Acad. Sci. USA* **109**, 5803–5808 (2012).
- Bosco, D. A. *et al.* Wild-type and mutant SOD1 share an aberrant conformation and a common pathogenic pathway in ALS. *Nat. Neurosci.* **13**, 1396–1403 (2010).
- Fang, C., Bourdette, D. & Banker, G. Oxidative stress inhibits axonal transport: Implications for neurodegenerative diseases. *Mol. Neurodegener.* **7**, 29 (2012).
- Rojas, F. *et al.* Reactive oxygen species trigger motoneuron death in non-cell-autonomous models of ALS through activation of c-Abl signaling. *Front. Cell. Neurosci.* **09**, 203 (2015).
- Fischer, L. R., Li, Y., Asres, S. A., Jones, D. P. & Glass, J. D. Absence of SOD1 leads to oxidative stress in peripheral nerve and causes a progressive distal motor axonopathy. *Exp. Neurol.* **233**, 163–171 (2012).
- Richardson, K. *et al.* The effect of SOD1 mutation on cellular bioenergetic profile and viability in response to oxidative stress and influence of mutation-type. *PLoS ONE* **8**, e68256 (2013).
- Jiang, X. *et al.* Challenges and opportunities for small-molecule fluorescent probes in redox biology applications. *Antioxidants Redox Signal.* **29**, 518–540 (2018).
- Tarpey, M. M., Wink, D. A. & Grisham, M. B. Methods for detection of reactive metabolites of oxygen and nitrogen: In vitro and in vivo considerations. *Am. J. Physiol. Regul. Integr. Comp. Physiol.* **286**, (2004).
- Okumoto, S. Imaging approach for monitoring cellular metabolites and ions using genetically encoded biosensors. *Curr. Opin. Biotechnol.* **21**, 45–54 (2010).
- Wolf, A. M., Nishimaki, K., Kamimura, N. & Ohta, S. Real-time monitoring of oxidative stress in live mouse skin. *J. Invest. Dermatol.* **134**, 1701–1709 (2014).
- Meyer, A. J. *et al.* Redox-sensitive GFP in *Arabidopsis thaliana* is a quantitative biosensor for the redox potential of the cellular glutathione redox buffer. *Plant J.* **52**, 973–986 (2007).
- Panieri, E., Millia, C. & Santoro, M. M. Real-time quantification of subcellular H<sub>2</sub>O<sub>2</sub> and glutathione redox potential in living cardiovascular tissues. *Free Radic. Biol. Med.* **109**, 189–200 (2017).
- Fujikawa, Y. *et al.* Mouse redox histology using genetically encoded probes. *Sci. Signal.* **9**, (2016).
- Du, Y., Hu, H., Pei, X., Du, K. & Wei, T. Genetically encoded FapR-NLuc as a biosensor to determine malonyl-CoA in situ at subcellular scales. *Bioconjug. Chem.* **30**, 826–832 (2019).
- Warren, L. & Lin, C. mRNA-based genetic reprogramming. *Mol. Ther.* **27**, 729–734 (2019).
- Duprez, J., Roma, L. P., Close, A. F. & Jonas, J. C. Protective antioxidant and antiapoptotic effects of ZnCl<sub>2</sub> in rat pancreatic islets cultured in low and high glucose concentrations. *PLoS One* **7**, (2012).
- Desireddi, J. R., Farrow, K. N., Marks, J. D., Waypa, G. B. & Schumacker, P. T. Hypoxia increases ros signaling and cytosolic Ca<sup>2+</sup> in pulmonary artery smooth muscle cells of mouse lungs slices. *Antioxidants Redox Signal.* **12**, 595–602 (2010).
- van Hameren, G. *et al.* In vivo real-time dynamics of ATP and ROS production in axonal mitochondria show decoupling in mouse models of peripheral neuropathies. *Acta Neuropathol. Commun.* **7**, 86 (2019).
- Gutscher, M. *et al.* Proximity-based protein thiol oxidation by H<sub>2</sub>O<sub>2</sub>-scavenging peroxidases. *J. Biol. Chem.* **284**, 31532–31540 (2009).
- Picher-Martel, V., Valdmanis, P. N., Gould, P. V., Julien, J.-P. & Dupré, N. From animal models to human disease: A genetic approach for personalized medicine in ALS. *Acta Neuropathol. Commun.* **4**, 70 (2016).
- Luigetti, M. *et al.* Heterozygous SOD1 D90A mutation presenting as slowly progressive predominant upper motor neuron amyotrophic lateral sclerosis. *Neurol. Sci.* **30**, 517–520 (2009).
- Holmøy, T., Wilson, J. A., Von Der Lippe, C., Andersen, P. M. & Berg-Hansen, P. G127R: A novel SOD1 mutation associated with rapidly evolving ALS and severe pain syndrome. *Amyotroph. Lateral Scler.* **11**, 478–480 (2010).
- Malakhova, A. A. *et al.* Generation of induced pluripotent stem cell lines ICGi021-A and ICGi022-A from peripheral blood mononuclear cells of two healthy individuals from Siberian population. *Stem Cell Res.* **48**, 101952 (2020).
- Ustyantseva, E. I. *et al.* Generation of an induced pluripotent stem cell line, ICGi014-A, by reprogramming peripheral blood mononuclear cells from a patient with homozygous D90A mutation in SOD1 causing Amyotrophic lateral sclerosis. *Stem Cell Res.* **42**, 101675 (2020).
- Das, A. T., Tenenbaum, L. & Berkhout, B. Tet-on systems for doxycycline-inducible gene expression. *Curr. Gene Ther.* **16**, 156–167 (2016).
- DeKaveler, R. C. *et al.* Functional genomics, proteomics, and regulatory DNA analysis in isogenic settings using zinc finger nuclease-driven transgenesis into a safe harbor locus in the human genome. *Genome Res.* **20**, 1133–1142 (2010).
- Ustyantseva, E. I. *et al.* A platform for studying neurodegeneration mechanisms using genetically encoded biosensors. *Biochemistry* **84**, 299–309 (2019).
- Du, Z.-W. *et al.* Generation and expansion of highly pure motor neuron progenitors from human pluripotent stem cells. *Nat. Commun.* **6**, 6626 (2015).
- Kotin, R. M., Linden, R. M. & Berns, K. I. Characterization of a preferred site on human chromosome 19q for integration of adeno-associated virus DNA by non-homologous recombination. *EMBO J.* **11**, 5071–5078 (1992).
- Jing, W. *et al.* Study of electrical stimulation with different electric-field intensities in the regulation of the differentiation of PC12 cells. *ACS Chem. Neurosci.* **10**, 348–357 (2019).
- Sirianni, A. C. *et al.* N-acetyl-L-tryptophan, but not N-acetyl-D-tryptophan, rescues neuronal cell death in models of amyotrophic lateral sclerosis. *J. Neurochem.* **134**, 956–968 (2015).
- Le Gall, L. *et al.* Molecular and cellular mechanisms affected in als. *J. Pers. Med.* **10**, 1–34 (2020).

43. Kruman, I. I., Pedersen, W. A., Springer, J. E. & Mattson, M. P. ALS-linked Cu/Zn-SOD mutation increases vulnerability of motor neurons to excitotoxicity by a mechanism involving increased oxidative stress and perturbed calcium homeostasis. *Exp. Neurol.* **160**, 28–39 (1999).
44. Sun, Y. H. *et al.* Human induced pluripotent stem cell line with genetically encoded fluorescent voltage indicator generated via CRISPR for action potential assessment post-cardiogenesis. *Stem Cells* **38**, 90–101 (2020).
45. Guha, S., Fischer, S., Johnson, G. V. W. & Nehrke, K. Tauopathy-associated tau modifications selectively impact neurodegeneration and mitophagy in a novel *C. elegans* single-copy transgenic model. *Mol. Neurodegener.* **15**, 65 (2020).
46. Sieger, D., Moritz, C., Ziegenhals, T., Prykhozij, S. & Peri, F. Long-range Ca<sup>2+</sup> waves transmit brain-damage signals to microglia. *Dev. Cell* **22**, 1138–1148 (2012).
47. Zhu, P. *et al.* Silencing and un-silencing of tetracycline-controlled genes in neurons. *PLoS ONE* **2**, e533 (2007).
48. Li, L., Chen, Y. & Gibson, S. B. Starvation-induced autophagy is regulated by mitochondrial reactive oxygen species leading to AMPK activation. *Cell. Signal.* **25**, 50–65 (2013).
49. Wengrod, J. *et al.* Phosphorylation of eIF2a triggered by mTORC1 inhibition and PP6C activation is required for autophagy and is aberrant in PP6C-mutated melanoma. *Sci. Signal.* **8**, 1–12 (2015).
50. White, E. S. Z. *et al.* Serum deprivation initiates adaptation and survival to oxidative stress in prostate cancer cells. *Sci. Rep.* **10**, 1–18 (2020).
51. Zhang, N. & Cao, L. Starvation signals in yeast are integrated to coordinate metabolic reprogramming and stress response to ensure longevity. *Curr. Genet.* **63**, 839–843 (2017).
52. Nicholls, D. G. & Budd, S. L. Mitochondria and neuronal glutamate excitotoxicity. *Biochim. Biophys. Acta Bioenerg.* **1366**, 97–112 (1998).
53. Van Damme, P. & Robberecht, W. Clinical implications of recent breakthroughs in amyotrophic lateral sclerosis. *Curr. Opin. Neurol.* **26**, 466–472 (2013).
54. Millecamps, S. & Julien, J. P. Axonal transport deficits and neurodegenerative diseases. *Nat. Rev. Neurosci.* **14**, 161–176 (2013).
55. Carriedo, S. G., Sensi, S. L., Yin, H. Z. & Weiss, J. H. AMPA exposures induce mitochondrial Ca<sup>2+</sup> overload and ROS generation in spinal motor neurons in vitro. *J. Neurosci.* **20**, 240–250 (2000).
56. Hsu, P. D. *et al.* DNA targeting specificity of RNA-guided Cas9 nucleases. *Nat. Biotechnol.* **31**, 827–832 (2013).
57. Jinek, M. *et al.* A programmable dual-RNA-guided DNA endonuclease in adaptive bacterial immunity. *Science* **337**, 816–821 (2012).
58. Medrano, R. F. V. & De Oliveira, C. A. Guidelines for the tetra-primer ARMS-PCR technique development. *Mol. Biotechnol.* **56**, 599–608 (2014).

## Acknowledgements

The authors thank the Microscopy Center of Biological Objects of the Siberian Branch of the Russian Academy of Sciences for granting access to microscopic equipment and SB RAS Genomics Core Facility for Sanger sequencing of the samples. We also thank Dana Frank (University of Groningen, Groningen, the Netherlands) for reading and language editing of the manuscript.

## Author contributions

E.U. and S.P.M. designed the research. E.U. performed the experiments (except for off-target analysis, co-localization imaging and XTT-assay) and analyzed the data. S.V.P. and A.A.M. performed co-localization imaging and XTT-assay, S.P.M. performed off-target analysis, K.U. wrote an image analysis macros and performed statistical analysis of the data, S.P.M. and S.M.Z. obtained the funding. E.U. drafted the manuscript and all authors revised and approved it. All authors have read and agreed to the published version of the manuscript.

## Funding

This work was supported by the State project of the Institute of Cytology and Genetics # FWNR-2022-0015.

## Competing interests

The authors declare no competing interests.

## Additional information

**Supplementary Information** The online version contains supplementary material available at <https://doi.org/10.1038/s41598-022-12807-z>.

**Correspondence** and requests for materials should be addressed to E.U. or S.P.M.

**Reprints and permissions information** is available at [www.nature.com/reprints](http://www.nature.com/reprints).

**Publisher's note** Springer Nature remains neutral with regard to jurisdictional claims in published maps and institutional affiliations.



**Open Access** This article is licensed under a Creative Commons Attribution 4.0 International License, which permits use, sharing, adaptation, distribution and reproduction in any medium or format, as long as you give appropriate credit to the original author(s) and the source, provide a link to the Creative Commons licence, and indicate if changes were made. The images or other third party material in this article are included in the article's Creative Commons licence, unless indicated otherwise in a credit line to the material. If material is not included in the article's Creative Commons licence and your intended use is not permitted by statutory regulation or exceeds the permitted use, you will need to obtain permission directly from the copyright holder. To view a copy of this licence, visit <http://creativecommons.org/licenses/by/4.0/>.

© The Author(s) 2022